Rabi-Oscillations-Induced Multiharmonic Emission in a Maxwell–Schrödinger Study of a Dense Sample of Molecules

ASHISH K. GUPTA, DANIEL NEUHAUSER

Department of Chemistry and Biochemistry, University of California, Los Angeles, California 90095-1569

Received 15 March 2000; revised 8 June 2000; accepted 8 September 2000

ABSTRACT: A solution of the combined Maxwell–Schrödinger equations for the propagation of an ultraviolet (UV) pulse in a sample of model H_2^+-like molecules (with only two electronic states), shows a significant increase of the emission at 5–10 harmonics for a thick-density (line integrated density of 50 a.u.$^{-2}$) vs. a thin-density case. The increase is more than two orders of magnitude larger than the expected factor (the ratio of the squared densities) and is due to a "sharpening" effect whereby Rabi oscillations induce a spatially rapidly varying electric field that has very sharp peaks. Equally important, the molecular degree of freedom is shown to exert a strong influence on the emitted radiation so that multiharmonic emission can be controlled by preparing molecules in specific initial wavepackets. © 2001 John Wiley & Sons, Inc. Int J Quantum Chem 81: 260–267, 2001

Key words: harmonic generation; Maxwell; Schrödinger; coherent; laser interactions

Introduction

When a strong laser pulse impinges on a molecule and causes electronic excitation, the resulting highly oscillatory dipole moment leads to emission of radiation at high frequencies. This phenomenon is called multiharmonic generation (HG). Typically, HG is studied theoretically for small systems in which the emission is a perturbation on the driving laser radiation. Most often, a single atom or molecule is studied theoretically (for early work see [1, 2]; for more recent work, see [3–7]), while experiments are typically done on a gas of sparsely spaced emitting molecules. The experiments and theoretical studies have established that HG can be very significant at high harmonics (extending beyond the 100th harmonic for He), due to strong scattering of the electrons, driven by the electric field, with the nuclear core. Another interesting effect found in studies of molecules in a strong field is selective ionization at a critical internuclear distance [8–11].

In this article we take the next step in HG studies, emission from an optically thick media. We ask what would be the effects of a high density of molecules on the HG spectrum. Specifically, when there

Correspondence to: D. Neuhauser; e-mail: dxn@chem.ucla.edu.

Contract grant sponsors: NSF, PRF, Alfred P. Sloan Fellowship.

is a sufficient density of molecules (an optically thick medium) the emission from these molecules is not a perturbation but becomes significant and affects the driving radiation. Thus, it is necessary to treat self-consistently the wave function of each emitting molecule together with the driving field.

For consistent treatment, we solve the combined Maxwell equation for the field and a Schrödinger equation for the molecules; in brief, a Maxwell–Schrödinger set of equations. If collisional deexcitation or spontaneous emission is important, it becomes necessary to represent the molecular degrees of freedom by a density matrix, and then the Schrödinger–Maxwell equations are replaced by a Maxwell–Bloch set. However, we consider here a very short pulse such that incoherent processes are negligible and the Maxwell–Schrödinger set is appropriate.

We note that there are several experimental and theoretical studies that are relevant for our problem. Recently, harmonic emission was studied from clusters and showed increased efficiency for HG emission. Another example is a recent study of a sparse collection of atoms or two-level systems (see, e.g., [12]) that has demonstrated a significant dependence of the emerging signal amplitude on the driving pulse width.

The Maxwell–Schrödinger equations are very computationally intensive, since a separate wave function needs to be included for each molecule along the fields' propagation axis. For this first study, we therefore consider an ultrasimplified model for coherent multiharmonic emission from molecules in which the molecules are placed in a small region of size a few hundred atomic units (a fraction of a single wavelength of the driving field). This region contains many molecules that absorb and emit simultaneously. We use a model associated with the simplest molecules, H_2^+, placing them on a one-dimensional (z) axis. The molecules are all aligned pointing along the x axis, so that rotation is not included. Upcoming works would include the possibility of random rotation of emitting molecules. The electric field propagates along the z axis and its polarization is along the molecular (x) axis. The most drastic simplification is that only two electronic states are considered per molecule. Thus, the model misses the effects of very high harmonics emission, which are dictated by electron–core scattering. However, the description at intermediate harmonics (up to 10–20) is the most important as far as the effects on the driving field, since emission is generally stronger at lower harmonics. An upcoming study [13] uses a better model for the electronic wave function.

We have several goals here. First, we study the effect of the emitting region's size. We show that increasing the size has dramatic effects on the HG spectrum. If the increase was just due to superradiance, i.e., coherent emission of all molecules at once based on the incoming field, we would have expected that the emitted intensity would increase quadratically with the number of molecules (as the polarization field would increase linearly with the number of coherently emitting molecules). However, the increase in HG with number of molecules is found to be higher than quadratic at high frequency. We show that it is due to an interesting phenomenon whereby the total electric field gets sharp cusps due to the interaction with the molecules. These sharp cusps are due to the fact that the polarization gets closely spaced peaks (spatial oscillations) that are due to Rabi oscillations. Specifically, at a given time molecules in different regions would feel the effects of the field differently. For example, there are regions with molecules that the pulse has just hit while others that have been passed already by the pulse. The amount of Rabi oscillation is different for the different molecules. Therefore, the propagation gets a spatial dependence (due to the spatial dependence of the Rabi oscillations). At the very strong fields we consider the spatial dependence of propagation leads to emission at short wavelengths.

Next we examine what are the effects of vibrationally exciting the molecular degree of freedom. In a previous work [14] we have shown that the harmonic emission profile for a single molecule depends strongly on vibrational excitation. We have further shown that the strong dependence of the emission on the vibrational excitation implies that for any desired spectral region, it is possible to prepare the molecule in an initial wavepacket that will lead to preferred emission in that range. In this study we show that even for multiple-molecule emission, there is a dependence of the emitted profile on the vibrational excitation. Thus, the emission profile could in principle be controlled by preparing the molecules in a specific wavepacket before the laser interacts with them.

The work is organized as follows. The next section gives a more detailed formulation of the problem, the third section discusses the results, which is followed by conclusions.

Formulation and Methodology

In this study, the noninteracting H_2^+-like model molecules are situated linearly on the z axis. No center of mass motion is allowed. Relative motion (vibrational motion) is allowed only in the x direction (i.e., perpendicular to z). The wave function of each molecule, situated at z, is formally then $\Psi(\mathbf{r}, x, z, t)$, where $\mathbf{r}$ is the electronic coordinate and x is the vibrational coordinate. This wave function is controlled by the Schrödinger Hamiltonian:

$$i\hbar\frac{\partial\Psi(\mathbf{r}, x, z, t)}{\partial t} = H\Psi(\mathbf{r}, x, z, t). \tag{1}$$

The Hamiltonian is

$$H = -\frac{\hbar^2}{2M}\frac{\partial^2}{\partial x^2} + H_{\mathrm{el}}(\mathbf{r}; x) - eE \cdot r_x, \tag{2}$$

where M is the reduced mass of H_2^+ and H_{el} is an electronic Hamiltonian that contains all the interaction potential terms (H_{el} has no explicit dependence on z). The last term is the laser molecule interaction (r_x is the x component of $\mathbf{r}$, and E is parallel to the x axis). The most important feature of (2) is that there is no kinetic term in z, so that the wave functions for each z are not mixed.

In the two-electronic state approximation, the wave function is

$$\Psi(\mathbf{r}, x, z, t) = \sum_{i=1}^{2} \kappa_i(\mathbf{r}; x)\psi_i(x, z, t), \tag{3}$$

where κ_i is the ith electronic state of the molecule, and it fulfills

$$H_{\mathrm{el}}\kappa_i(\mathbf{r}; x) = V_i(x)\kappa_i(\mathbf{r}; x), \tag{4}$$

where V_i are the Born–Oppenheimer potentials for this problem. The two-electronic state approximation, while crude at the intensities considered (up to 10^{17} W/cm^2), is motivated, as mentioned above, by our desire to concentrate on the molecular degree of freedom. (A description of very high harmonics would necessitate a more proper description of the electronic wave function and its motion near the core.) The two-electronic-state analysis should be sufficient to obtain generic features for other types of systems for which two electronic states are dominant, as well as lower intensity situations, in spite of the omission of the ionizing component and the core–electron scattering. More quantitative studies using a larger electron basis would be pursued in future calculations, but the features found in this study (electric field and polarization field cusps, Rabi oscillation effects, and dependence on vibrational states) should be generic.

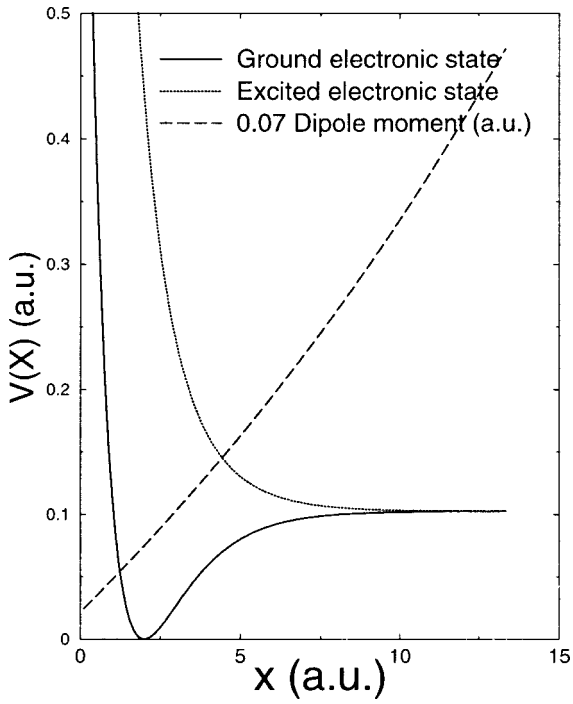

FIGURE 1. Static potential curves for H_2^+ (ground and excited, in a.u.) and the linearly rising dipole moment (multiplied by 0.07), as a function of the distance between the atoms.

Substituting Eqs. (3) and (4) in Eqs. (1) and (2), we eventually get the final set of Schrödinger equations:

$$i\hbar\frac{\partial\psi_j(x, z, t)}{\partial t} = -\frac{\hbar^2}{2M}\frac{\partial^2\psi_j(x, z, t)}{\partial x^2} + V_j(x)\psi_j(x, z, t) - \sum_{i=1}^{2}\mu_{j,i}(x)E(z, t)\psi_i(x, z, t), \tag{5}$$

where μ_{ij} is dipole moment

$$\mu_{ji}(x) = \langle\kappa_j(r; x)|e\mathbf{r}_x|\kappa_i(r; x)\rangle. \tag{6}$$

Figure 1 shows the ground ($j = 1$) and first excited ($j = 2$) potentials for H_2^+, which are bound and repulsive, respectively, as well as the off-diagonal dipole coupling, which rises linearly with distance.

In addition to the Schrödinger equation, we need to consider the Maxwell equations for the laser field. One simplification is that we consider only the polarization contributions and ignore the current density (i.e., the magnetic dipole moment). The Maxwell equations are then given below:

$$\frac{1}{c}\frac{\partial D}{\partial t} = \frac{\partial B}{\partial z}, \tag{7}$$

$$\frac{1}{c}\frac{\partial B}{\partial t} = \frac{\partial E}{\partial z}, \tag{8}$$

where B is the magnetic field, the displacement vector is $D = E + 4\pi P$, while the polarization is

$$P(z,t) = \rho(z) \int \psi_1^*(x,z,t)\mu_{1,2}(x)\psi_2(x,z,t)\,dx + \text{c.c.} \tag{9}$$

The Schrödinger and Maxwell equations are connected here through P and E. P is defined in terms of the molecular wavepacket but appears in the Maxwell equations, and E also appears in both equations.

The final set of equations is then Eqs. (5), (7), and (8). Together, these equations are of an initial value form, so that from the values of the wave function and electric field at $t = 0$ we can find the values at any later time.

Numerically, the Maxwell–Schrödinger equations, Eqs. (5), (7), and (8), are solved by a very simple fifth-order Runge–Kutta algorithm. The method is straightforward. We discretize a long grid containing N_z points for $E(z,t)$ and $B(z,t)$,

$$z = z_0 + j * dz, \qquad j = 0, \ldots, N_z.$$

The molecular wave function $\psi_j(x,z,t)$ is represented on a two-dimensional x–z grid (see Fig. 2):

$$z = z_0 + j * dz, \qquad j = j_s, \ldots, j_s + L_z, \tag{10}$$

$$x = x_0 + i * dx, \qquad i = 0, \ldots, N_x, \tag{11}$$

where j_s and L_z are the starting point and the number of grid points in the z direction for the wave function part. L_z is much smaller than N_z, since we assume that the molecules are placed on a small (subwavelength) region.

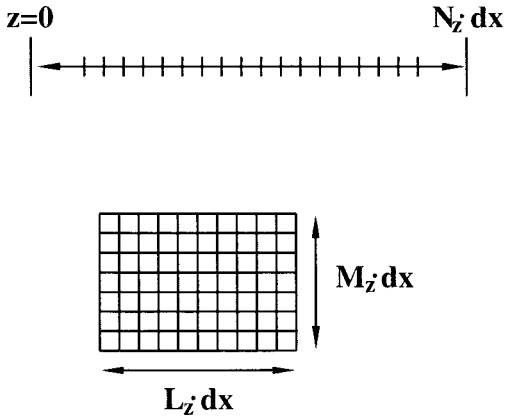

FIGURE 2. Schematic representation of the grids employed a long one-dimensional grid for $E(z,t)$ and a small two-dimensional grid for $\psi_j(x,z,t)$.

The main ingredient fed into the Runge–Kutta propagation is a routine into which we input the instantaneous values of $E(z,t)$ and $B(z,t)$ along the long grid and the values of $\psi_j(x,z,t)$ and which outputs the values of $\partial E/\partial t$, $\partial B/\partial t$, and $\partial \Psi/\partial t$. The calculation of the time derivatives is straightforward. It necessitates the spatial derivatives of B and E, which are calculated by a simple five-point formula, and in Eq. (5) the spatial derivatives in x are calculated by an DVR-FT-based formulas [15]. We tested different methods for calculating the derivatives and settled on this combination for improved efficiency.

Results

DENSITY DEPENDENCE

Our first goal was investigating the dependence on the emitted radiation on the density and total number of emitting molecules. For this purpose we used a Gaussian density profiles. Two profiles were used; a thick and a thin density (although even the "thick" density extends over a less than a fundamental's wavelength). The thick density was

$$\rho(z) = \rho_{\max} \exp\left[-(z - z_0)^2/2a^2\right], \tag{12}$$

where $\rho_{\max} = 0.1$ (a.u.)$^{-3}$, $z_0 = 18{,}750$ a.u., and $a = 200$ a.u. The thin density was

$$\overline{\rho}(z) = \overline{\rho}_{\max} e^{-(z-z_0)^2/2\overline{a}^2}, \tag{13}$$

where $\overline{\rho}_{\max} = 0.18$ (a.u.)$^{-3}$ and $\overline{a} = 7$ a.u. The line integral of this density is significantly smaller than that of $\rho(z)$:

$$\int \overline{\rho}(z)\,dz = 1 \text{ (a.u.)}^{-2},$$

$$\int \rho(z)\,dz = 49.5 \text{ (a.u.)}^{-2}. \tag{14}$$

The reason for using an artificially smooth Gaussian density (rather than using, e.g., a slab density) was to ensure that our final results are due to genuine strong-field effects and not due to reflection from any edges of a slab.

An $N_z \times dz = 8000 \times 10$ a.u. grid was employed for the electric and magnetic fields, with fewer points in z ($L_z = 250$) for representing the molecular wavepacket. For x, an 121×0.11 a.u. grid was used.

The initial field profile was a wide-frequency (narrow spatial extent) Gaussian-like ultraviolet

(UV) pulse of duration ≈3 fs:

$$E(z,\ t=0) = E_0 e^{-z^2/2\sigma^2}\left[-\frac{w_0}{c}\cos\left(\frac{w_0}{c}z\right) - \sin\left(\frac{w_0}{c}z\right)\frac{zw_0}{\sigma^2}\right], \quad (15)$$

where $\sigma = 1440$ a.u. The maximum intensity was at $\hbar\omega_0 = 0.43$ a.u., i.e., a wavelength $\lambda_0 = 2000$ a.u. This field is very wide in spectral content and approximately resonant with the Franck–Condon transition frequency. A strong field was employed, with the E_0 coefficient adjusted so that the maximum amplitude was 1 a.u., i.e., a maximum intensity of 1.4×10^{17} W/cm^2. The pulse is thus extremely intense and causes significant excitation to the excited state (i.e., it has a large "area"). For real molecules (if the two-state approximation is not used) this field would cause much ionization.

We first examine the emission in the thick-density case. Figure 3 shows the electric field (solid line) at different times. Initially the electric pulse is just entering the molecular interaction region. Then the pulse is inside the region and is modified, and finally the pulse is just leaving the region. The incoming pulse is smooth but the outgoing pulse has sharp cusps. We have checked that the cusps are real and are not spurious effects of the discreteness of the grid, i.e., our simulations are converged even in the presence of the sharp cusps. (The simulations were repeated with the original grid spacing, 10 a.u., and with a finer grid spacing, 3.333 a.u., yielding identical results.) Figure 3 also shows the polarization (dotted line) at different times. The polarization is discussed below.

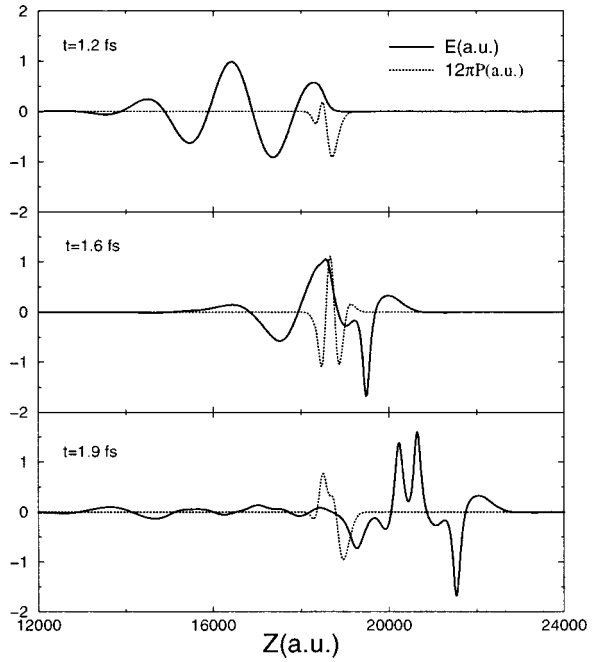

FIGURE 3. Electric field and polarization at different times. At $t = 1.2$ fs the laser pulse is just approaching the molecular interaction region, at $t = 1.6$ fs the pulse is inside the interaction region, and at $t = 1.9$ fs the major part of the pulse has left the interaction region.

Figure 4 shows the energy density of the emergent electric and magnetic fields, defined here as $(|E(\omega)|^2 + |B(\omega)|^2)/8\pi$, where $E(\omega)$ is the spectral component of the emergent electric field as measured at large (positive) values of z. (Approximately a quarter of the pulse energy reflects back toward the negative z region, but the reflected part has very few multiharmonic components.) It is clear

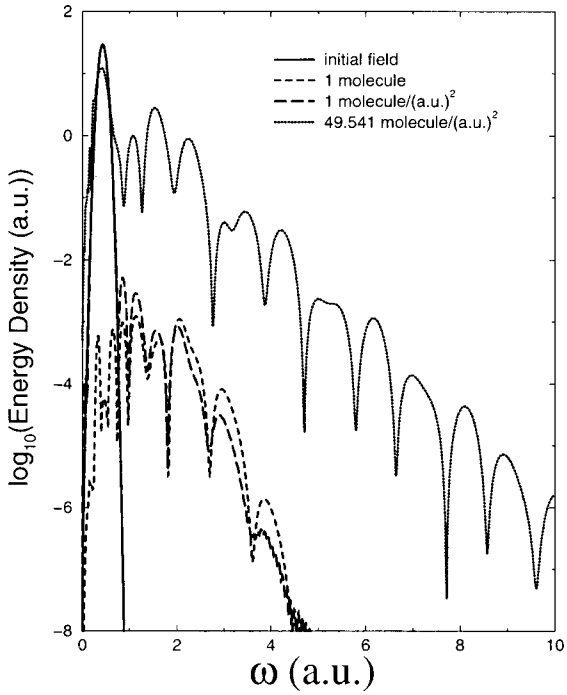

FIGURE 4. Energy density of the emitted electric and magnetic fields, $(|E(\omega)|^2 + |B(\omega)|^2)/8\pi$, calculated at large z where the particle density is already vanishing. Shown are the emergent spectra for the thick- and thin-density cases, as well as the initial field profile. The $\approx 10^3$–10^4 ratio in harmonic generation efficiency at frequencies up to 2 a.u. is due to the N^2 coherent emission factor (2500 here), while at higher frequencies (2–4 a.u.) the ratio between the emission intensities becomes larger than 10^5. On the same graph we also have power spectra of one molecule calculated directly from time-dependent polarization.

that much of the pulse energy was converted to emission at higher frequencies.

We now turn to a comparison between the thick and thin density cases. As Figure 4 shows, the emission for the thin density is significantly lower in magnitude. (We verified that the exact details of the thin density are not important, only the line integral, provided the width $\bar{a}$ is sufficiently small.) Equally important, the emission spectrum falls off much more rapidly in the thin-density case than in the thick-density case.

The reasons for the different emission profiles for the two densities are twofold. The obvious reason is the increase in the number of emitting molecules, which increases the polarization by N^2, where N is the ratio in effective number contributing, i.e., the ratio of the integrated densities. Here N^2 is approximately 2500, which gives the order of magnitude of the ratio of intensities up to frequencies of $\approx$2 a.u. (see Fig. 5). However, beyond 2 a.u. the emission in the thin-density case falls off more rapidly with frequency, while the emission in the thick-density case falls off only slowly. The typical ratio between the emission amplitudes becomes 10^5 or larger (Fig. 5).

The intense emission profile for the thick density is related to the sharp peaks in the emitted electric field [$E(t)$]. In the high-density case shown in Figure 3 and in more detail in Figure 6, the evolution and origin of the cusps is quite interesting. The main clue to the specifics of the cusp emission is the polarization at short time (Figs. 3 and 6). This polarization has a shorter wavelength than the electric field. As mentioned, the spatial oscillations of the polarization at short times are not due directly to the frequency of the field, but are Rabi oscillations. To see that, we show in Figure 6 the population, as a function of position, which clearly shows the Rabi oscillations in the polarization and the population.

For very high frequencies (above 4 a.u., i.e., above the 10th harmonic), the ratio between the emission for the thick and thin densities should start decreasing, eventually becoming of order N (incoherent emission) or less, since the high-frequency

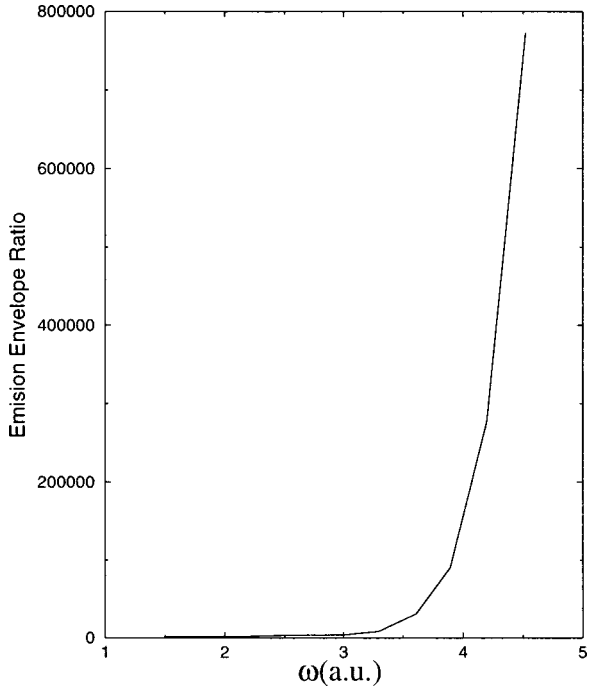

FIGURE 5. Ratio of the envelope of the emission intensities for thick and thin densities as a function of frequency. At 2–4 a.u. the initial N^2 ($\simeq$2500) superradiance emission mechanism is dominant, while at later frequencies the ratio grows due to the cusps that lead to long tails in the frequency-dependent emission profile.

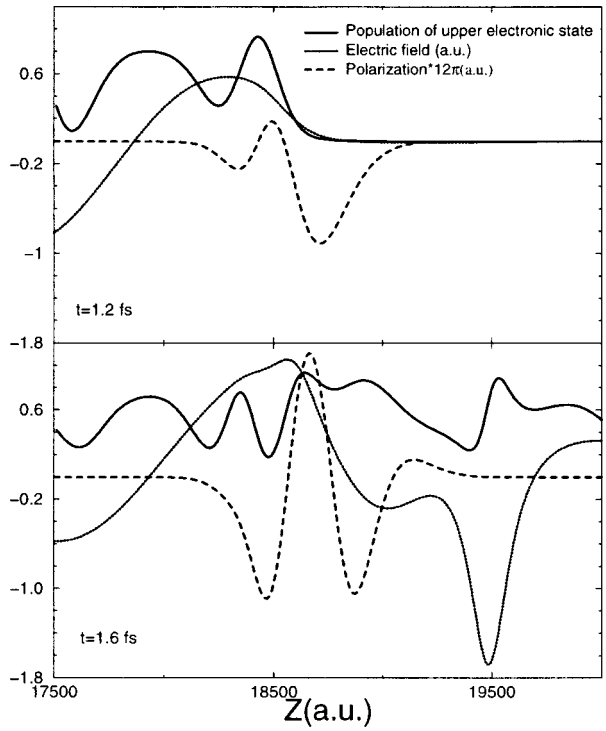

FIGURE 6. Effects of Rabi oscillations on the electric field at different times. (Note the similarity to Fig. 3 but the different length scale, covering only the region with the molecules.) The population at short times exhibit spatial Rabi oscillations, which involve similar oscillations in the polarization. These then cause (second panel) oscillation in the electric field.

harmonics have wavelengths that are comparable to or smaller than the size of the emitting region. However, the energy density is so small for high frequencies that we cannot trust the numerical results and have therefore not plotted results with energy density below 10^{-8} a.u.

Emission from a Single Molecule

To check the consistency of the calculation, we compared the thin-density case with the emission spectrum from one molecule. The emission spectrum is calculated from

$$I(\omega) \propto \omega^4 \left| \int_0^\infty e^{i\omega t} P(t)\, dt \right|^2, \qquad (16)$$

where the polarization is calculated here by solving Schrödinger's equation for the wave function subject to the original electric field. The polarization is directly used to calculate the emission spectrum. The emitted intensity [$I(\omega)$] does not contain the contribution of the original pulse to the radiation intensity, which is contained automatically in the calculation of the transmitted intensity in the Maxwell–Schrödinger equation. Therefore, at low frequencies the thin-density and single-molecule curves do not overlap; however, at higher frequencies where the spectral content of $E_0(\omega)$ is small, the thin-density and single-molecule spectra agree completely.

Effects of Vibrational Excitation

Next we examine (for the thick-density case) the role of the molecular degree of freedom, the H–H distance (x). Specifically, we study the effects of vibrationally exciting the molecules or alternately fixing them (fixing x by setting the molecular mass to be $M = \infty$). As shown in Figure 7, the simulations give qualitatively similar results. However, the peak positions and heights are very different, and the order varies with the vibrational state. (Qualitatively, the system samples a large number of Floquet states, associated with different frequencies, and the coefficients associated with the Floquet states vary depending on the initial molecular state.) Physically, the effective potential energy difference (excited-ground) sampled by the first vibrational eigenstate has a big spread, especially stretching toward larger x, i.e., lower values of the energy difference. This can explain why there is depletion of the low-frequency field for the first vibrationally excited state as it is converted to higher frequencies.

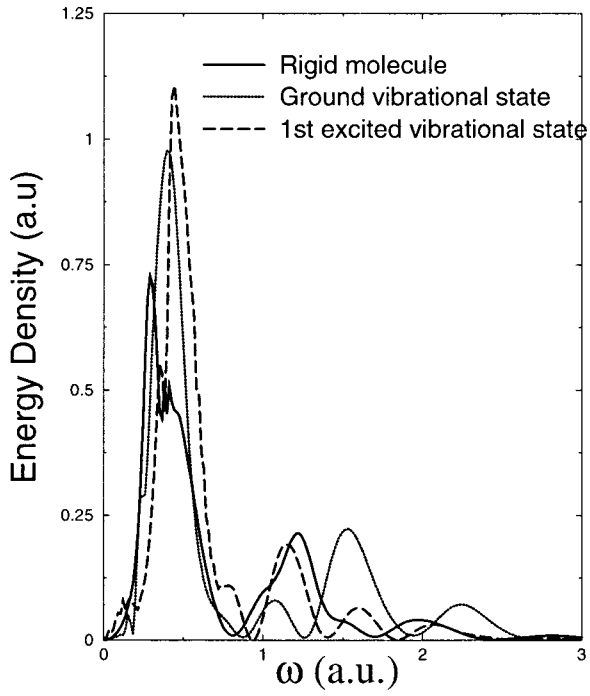

FIGURE 7. Spectrum of the emergent electric fields, for ground and excited initial H_2^+ vibrations and for a rigid molecule (obtained by setting $M = \infty$).

The results of Figure 7 show that, in principle, one can envision the following approach [14, 16] toward controlling the spectra of emitted multiharmonic radiation: first letting a long-time well-defined laser pulse impinge on a sample causing large-scale vibrational excitation, which in turn causes a specific multiharmonic emission profile when the strong pulse is turned on. (For other approaches for controlling emission using a mixture of strong and weak lasers see, e.g., [4]; for the use of a prebuilt molecular symmetry to build specific emission at the specified harmonics see [17].)

Wavepacket Evolution

Finally, Figure 8 shows the evolution of the wave function, for the thick-density case and with all molecules initially in a vibrationally excited state. Specifically, the figure shows $|\Psi^2|$ on the ground and upper electronic states, for a diatom placed at $z = z_0$. The most notable feature is that there are times where a very large portion of the wave function is on the repulsive state, but eventually most of it returns to the ground state so that most molecules have not been dissociated. This is a general

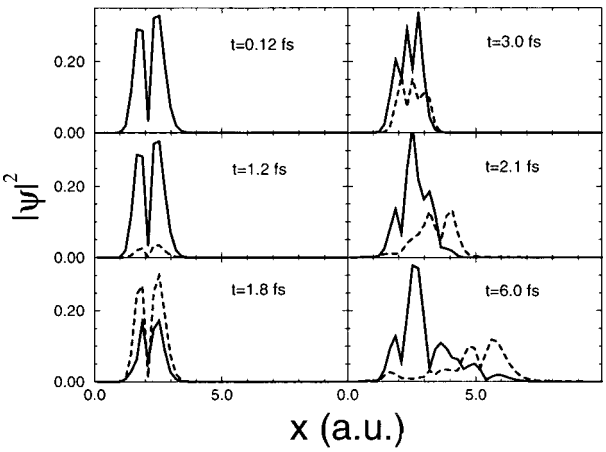

FIGURE 8. Evolution of the wavepacket density $|\psi_j(x,z,t)|^2$ for the maximum density point ($z = z_0$). The solid and dashed lines denote the population on the ground and excited electronic surfaces. The initial wavepacket is on the first excited vibrational state. Note the Rabi oscillation at $t = 1.2$ fs.

feature (found also when the molecules are initially in the ground vibrational state) and is due to the steepness of the excited-state potential, which leads to destructive interference of the components on the excited state. In addition, even at long times the wave functions on the upper and ground states overlap; however, the resulting dipole is too weak to cause significant modification of the emission spectrum, so that by $t = 7.2$ fs the fields' spectra are set.

Conclusions

In conclusion, with a slab of molecules less than a micron in thickness, it is predicted that multiharmonic emission will be very powerful, both due to coherent multiparticle emission as well as the presence of sharp features in the electric field caused by Rabi oscillations in the propagation. The multiharmonic emission could be in principal controlled by changing the initial molecule profile or even by making an appropriate initial coherent wavepacket combination [16] of different vibrations [14], as will be examined in future studies. Other future goals are the inclusion of higher lying electronic states (for better treatment of higher harmonics and ionization) for the molecular problem. Since this work does not treat core–electron scattering, which is responsible for the long tail of the multiharmonic generation, it cannot be directly applicable to predict a large magnitude of multiharmonic emission in strong fields, but the effects found (cusps, increased tail, and dependence on vibrational state) should be relevant in general.

ACKNOWLEDGMENTS

We are grateful to Ronnie Kosloff and Nimrod Moiseyev for helping stimulate our interest in this field, and to Roi Baer for reviewing the manuscript. One of us (A.K.G.) is grateful to Manoj K. Mishra for a helpful discussion. The research was supported by the NSF and the PRF foundations and by an Alfred P. Sloan Fellowship.

References

1. Bunkin, F. V.; Tugov, I. I. Phys Rev A 1973, 8, 601.
2. For a comprehensive review of works prior to 1991, see articles in J Opt Soc Am B 1990, 7, 403–688.
3. Krause, J. L.; Schafer, K. J.; Kulander, K. C. Phys Rev Lett 1992, 68, 3535.
4. Zuo, T.; Bandrauk, A.; Ivanov, M.; Corkum, P. B. Phys Rev A 1995, 51, 3991.
5. Tong, X.-M.; Chu, S.-I. Phys Rev A 1998, 58, 2656.
6. Kopold, R.; Becker, W.; Kleber, M. Phys Rev A 1998, 58, 4022.
7. Moiseyev, N.; Chrysos, M.; Atabek, O.; Lefebvre, R. J Phys B 1995, 28, 2007.
8. Cornaggia, C.; Normand, D.; Morellec, J. J Phys B 1992, 25, L415.
9. Hatherly, P. A.; Stankiewicz, M.; Codling, K.; Frasinski, L. J.; Cross, G. M. J Phys B 1994, 27, 2993.
10. Chelkowski, S.; Zuo, T.; Atabke, O.; Bandrauk, A. D. Phys Rev A 1995, 52, 2977.
11. Seideman, T.; Ivanov, M. Yu.; Corkum, P. B. Phys Rev Lett 1995, 75, 2819.
12. Chrystov, I. P.; Murnane, M. M.; Kapteyn, H. Phys Rev A 1998, 57, 2285.
13. Gupta, A. K.; Neuhauser, D., to be submitted.
14. Gupta, A. K.; Neuhauser, D. Chem Phys Lett 1998, 290, 543.
15. Marston, C. C.; Ballint-Kurti, G. G. J Chem Phys 1989, 91, 3571.
16. Watson, J. B.; Sanpera, A.; Chen, X.; Burnett, K. Phys Rev A 1996, 53, 1962.
17. Alon, O. E.; Averbukh, V.; Moiseyev, N. Phys Rev Lett 1998, 80, 3743.